Cerebral Cortex October 2015;25:3673–3681
doi:10.1093/cercor/bhu221
Advance Access publication September 21, 2014

Vascular Supply of the Cerebral Cortex is Specialized for Cell Layers but Not Columns

Daniel L. Adams[1,2], Valentina Piserchia[2], John R. Economides[1] and Jonathan C. Horton[1]

[1]Beckman Vision Center, University of California, San Francisco, San Francisco, CA 94143, USA and [2]Center for Mind/Brain Sciences, The University of Trento, Trento, Italy

Address correspondence to Jonathan C. Horton, PhD, Beckman Vision Center, University of California, San Francisco, 10 Koret Way, San Francisco, CA 94143-0730, USA. Email: hortonj@vision.ucsf.edu

The vascular supply to layers and columns was compared in macaque primary visual cortex (V1) by labeling red blood cells via their endogenous peroxidase activity. Alternate sections were processed for cytochrome oxidase to reveal "patches" or "blobs," which anchor the interdigitated column systems of striate cortex. More densely populated cell layers received the most profuse blood supply. In the superficial layers the blood supply was organized into microvascular lobules, consisting of a central venule surrounded by arterioles. Each vessel was identified as an arteriole or venule by matching it with the penetration site where it entered the cortex from a parent arteriole or venule in the pial circulation. Although microvascular lobules and cytochrome oxidase patches had a similar periodicity, they bore no mutual relationship. The size and density of penetrating arterioles and venules did not differ between patches and interpatches. The red blood cell labeling in patches and interpatches was equal. Moreover, patches and interpatches were supplied by an anastomotic pial arteriole system, with no segregation of blood supply to the two compartments. Often a focal constriction was present at the origin of pial arterial branches, indicating that local control of cortical perfusion may be accomplished by vascular sphincters.

Keywords: cytochrome oxidase blob, fMRI, macaque visual cortex, microvascular lobule, microvascular sphincter

Introduction

Although it weighs only a few pounds, the human brain consumes ~20% of the heart's output (Lawrence 1819; Kety 1948). Given its voracious demand for energy, one would expect the brain to have a vascular supply coupled precisely to the activity of its neurons. In the cerebral cortex, neurons are assembled into a functional architecture comprised of horizontal layers and vertical columns (Hubel and Wiesel 1977; Mountcastle 1997). The main goal of this study was to compare how the cortex's vascular supply is organized to satisfy the metabolic requirements of neurons in layers and columns.

The primary visual cortex (striate cortex, V1) has a particularly elaborate functional architecture, with multiple, interdigitated column systems serving different receptive field properties, such as ocular dominance, orientation, and spatial frequency (Hubel and Wiesel 1969; Hubel et al. 1978; Tootell et al. 1981; Bonhoeffer and Grinvald 1991; LeVay and Nelson 1991; Hübener et al. 1997; Issa et al. 2000; Swindale et al. 2000; Ts'o et al. 2009). A striking example of its modular architecture has been revealed in tangential sections processed for cytochrome oxidase (CO) (Wong-Riley 1979). The mitochondrial enzyme forms a regular array of columns, each a vertical cylinder of constant size extending through all layers except 4a and 4c (Horton and Hubel 1981). Known as CO "patches" or "blobs," these structures fit into precise register with other column systems, such as those representing ocular dominance.

In striate cortex, energy utilization reflected by CO levels is known to be correlated with neuronal spike rates (DeYoe et al. 1995). Recordings from implanted multielectrode arrays have shown that cells within CO patches have a 49% higher mean rate of spike discharge compared with cells located in interpatches (Economides et al. 2011). It has remained controversial, however, whether CO patches have a richer blood supply than surrounding cortex, in order to meet their cells' greater energy requirements (Zheng et al. 1991; Keller et al. 2011).

This issue is related closely to the broader question of whether the microvascular supply of the cerebral cortex is organized in coordination with its columnar architecture (Harel et al. 2010). In humans the ocular dominance columns in V1 are relatively large and can be mapped readily using functional magnetic resonance imaging (fMRI) (Cheng et al. 2001). Mapping the orientation columns is more difficult (Sun et al. 2013). Kamitani and Tong (2005) found that when subjects viewed gratings at 8 possible orientations, one could determine which orientation was being displayed by analyzing the pattern of fMRI activity in striate cortex, even at a spatial resolution of $3 \times 3 \times 3$ mm. This finding is surprising, when one considers that human orientation columns are probably much smaller than voxels of that size. One would expect the signal generated by orientation columns corresponding to the stimulus to be swamped by the global cortical response (Logothetis and Wandell 2004). To explain this result, Gardner (2010) has proposed that functional vascular units might be arranged in a special fashion with respect to columnar maps. For example, regions of striate cortex favoring a given orientation might be perfused by penetrating arterioles all derived from the same parent artery as it meanders across the pial surface. If so, weak fMRI signals would be detectable by changes occurring in blood oxygenation levels in an ensemble of vessels supplying columns of the same orientation over a wide region of cortex. To address this matter, at least indirectly, we examined whether CO patches and interpatches are supplied by the same or different pial arterial circulations.

Materials and Methods

Experiments were conducted in 2 Rhesus monkeys obtained from the California National Primate Research Center, Davis, CA. Monkey 1 was a 1-year-old female and Monkey 2 was a 12-year-old female. The animals were used for unrelated experiments by other investigators who donated the brains to our laboratory. Procedures were approved by the Institutional Animal Care and Use Committee at the University of California, Davis.

Each animal was placed under general anesthesia with ketamine HCl (20 mg/kg, i.m.) and killed with an intravenous injection of pentobarbital (150 mg/kg). The volume of pentobarbital solution required to produce rapid cardiac arrest was only 0.5 mL for Monkey 1 and 2.0 mL for Monkey 2. Therefore, intravenous euthanasia did not dilute red blood cells in the cerebral circulation. After death, 3 h were allowed to

elapse for intravascular coagulation of red cells. The brain was then extracted in an unperfused, unfixed condition. The operculum was removed from each occipital lobe by slipping a spatula into the calcarine fissure and slicing horizontally. The opercular blocks, measuring ~25 × 25 mm with a thickness of 4 mm, were placed into 2% paraformaldehyde with 30% sucrose in 0.1 M phosphate buffer solution (PBS), pH 7.4, and left for 2 days at room temperature. To avoid squeezing red blood cells out of the tissue, the blocks were not flat-mounted or placed under weights. After they had sunk, tangential sections were prepared on a freezing microtome. The first section was cut at 150 μm and processed for endogenous peroxidase activity to visualize the arterial and venous pial vascular systems. Thereafter, alternating sections were cut either for CO (30 μm) or endogenous peroxidase activity (150 μm). Peroxidase sections were collected in 0.1 M PBS whereas CO sections were slide-mounted immediately and air dried.

To label endogenous peroxidase activity in red cells, free-floating 150 μm sections were incubated in 3,3′-diaminobenzidine tetrahydrochloride hydrate (DAB) (0.5 mg/ml) dissolved in 0.1 M PBS. After 25 min the sections were transferred to a solution containing the same concentration of DAB with 0.01% H_2O_2. After reacting for 15 min, the sections were rinsed in PBS and mounted on slides. The other set of sections was processed for CO activity as described previously (Sincich and Horton 2005).

There were 2 key elements to our approach. First, to assess the blood supply of the cortex, the brain was not perfused. Instead, erythrocytes were labeled by relying upon their endogenous peroxidase activity to catalyze the oxidation of DAB (Kapralov et al. 2009). The resulting reaction product reflected the distribution of red cells within the brain parenchyma at the time of death. This method gives similar results to those acquired by perfusing *postmortem* with india ink, gelatin, latex, or methyl methacrylate resins to fill the vascular system (Duvernoy et al. 1981). Second, we identified the circular profiles of blood vessels in tangential sections as arterioles or venules by matching each one to its vessel of origin running along the pial surface. This overcame a major obstacle, namely, that one cannot easily differentiate arterioles from venules within a tissue section of cerebral cortex processed using standard histological stains. Recently, a number of specific labels have been proposed to distinguish arterioles from venules (dela Paz and D'Amore 2009; Atkins et al. 2011; Marcelo et al. 2013). For example, Alexa Fluor 633 labels cortical arterioles by binding to elastin (Shen et al. 2012). However, no easy marker is available yet for veins. Fortunately, the arteries and veins running along the pial surface are easy to tell apart. Therefore, when cutting the tissue block on the microtome the first section containing the pial vascular system was carefully preserved. This section was examined at 200× in a Zeiss Axioskop and the arterial and venous vascular systems were drawn with the aid of a camera lucida attachment. The site where each daughter vessel issued from a parent pial vessel and penetrated the cortex was identified and matched to a corresponding blood vessel in the next tissue section. Each vessel was then traced serially from section to section to identify each major circular profile in layer 3 as either an arteriole or venule. Other laboratories have used the surface pial vasculature in a similar fashion to align optical images of intrinsic signals with the blood vessels in tangential sections of primary visual cortex (Yoshioka et al. 1996; Xu et al. 2004; Lu and Roe 2008; Valverde Salzmann et al. 2012).

Digital photographs were taken with a SPOT RT color CCD camera (Diagnostic Instruments) mounted on an Olympus SZH10 microscope or a Zeiss Axioskop microscope. To define the patches, images were imported into PhotoShop CS6 (Adobe Systems, San Jose, CA). The holes from blood vessels were filled in with pixels of the local mean grayscale value using the "dust and scratches" filter tuned to the largest vessel diameter. This step prevented dark or bright pixels corresponding to blood vessels from influencing the division of CO into different zones based on staining intensity. Dark pixels were present if blood clot remained in the blood vessel. Bright pixels were present if blood had washed out of the vessel lumen, leaving it empty. This occurred frequently in the CO sections, owing to the fact that they were relatively thin and immersed in liquid for ~ 12 h during the CO reaction.

To compensate for unevenness in CO density due to fluctuation in section depth between layer 2 (lighter CO) and layer 3 (darker CO), a region-by-region normalization of image contrast was performed using MATLAB's (MathWorks, Natick, MA) Contrast-Limited Adaptive Histogram Equalization function ("adapthisteq"), available in the image analysis toolbox. This step is important, because otherwise image thresholding will produce smaller patches in layer 2 than in layer 3. The operation divides the image into tiles and matches the histograms of pixel values. Neighboring tiles are then recombined using bilinear interpolation to eliminate their boundaries. The resulting image was blurred with a Gaussian filter ($\sigma = 20$ μm) to smooth luminance borders. Isodensity contours were placed on the image to divide it into 6 zones of equal area. The darkest 2 zones enclosed by isodensity contours, corresponding to 33% of the surface area, were defined as CO patches (Purves and LaMantia 1993; Farias et al. 1997; Sincich and Horton 2005).

Contours representing the CO patches were superimposed on an image of an adjacent DAB-processed section. Precise alignment was achieved by matching the blood vessels in the adjacent CO and DAB sections. A rigid size transformation (~4%) was applied to the DAB section to compensate for slight shrinkage that occurred during histological processing. The number of arterioles and venules in the DAB section located in patches versus interpatches was counted. A chi-square (χ^2) test was used to determine if the vessel distribution differed significantly from a random distribution.

The total red blood cell content of patches versus interpatches was compared. The grayscale density values of the pixels comprising the DAB image ranged from 0 (black) to 255 (white). These values were summed separately for all pixels located within patches and interpatches. The absolute numbers were arbitrary, because they depended on image resolution, brightness, and contrast. However, their ratio reflected faithfully the proportion of red blood cells in patches versus interpatches.

Blood vessel diameters were measured in DAB-stained sections by fitting an ellipse to the border of each lumen. The minor axis was taken as the vessel diameter, to account for the fact that the plane of tangential section was sometimes slightly oblique with respect to the vessel lumen (Keller et al. 2011). Identification of blood vessels as arterioles or venules, plotting of their location, and measurement of their diameter were all performed in DAB-processed sections by an investigator blind to the location of the CO patches. After these steps were performed, comparison was made with the patches in adjacent CO-processed sections.

Results

Laminar Perfusion of the Cortex

In animals that have undergone cardiac perfusion with fixative solutions the cortex is virtually transparent in DAB-processed sections, except for the occasional stray red blood cell. In contrast, the cortex stains darkly in unperfused animals. The peroxidase labeling represents the combined red cell load in arterioles, capillaries, and venules. In the primary visual cortex, the strongest peroxidase signal was present in layers 6 and 4c (Fig. 1). In contrast, labeling was weak in layers 5 and 4b, and nearly absent in layer 1. Layer 2/3 showed an intermediate level of peroxidase staining. Layer 4a, a 50 μm leaflet of cortex sandwiched between layers 4b and 3, had no recognizable counterpart in sections reacted for peroxidase activity. Furthermore, no distinction could be made between the red blood cell signal in layer 4cβ (parvocellular) versus layer 4cα (magnocellular). These 2 exceptions aside, the distribution of red blood cells matched the density of neurons in the horizontal layers of the cortex. This finding implies that the blood supply to the cortex is coupled tightly to the metabolic demands of the neurons populating each layer (Weber et al. 2008).

Microvascular Lobules of the Cortex

In sections cut tangentially to the pial surface, large clot-filled blood vessels were visible to the naked eye in layer 2/3 (Fig. 2). Each vessel was surrounded by a dark halo of

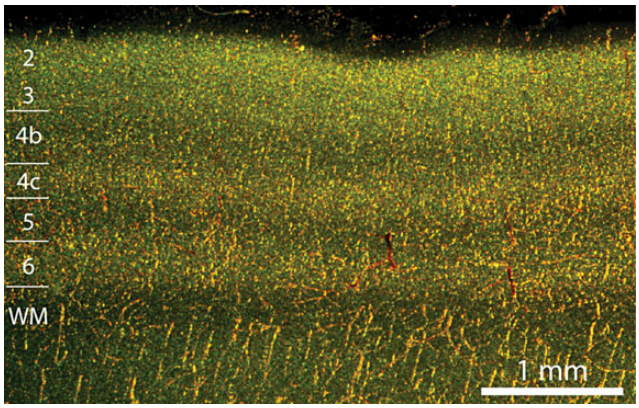

Figure 1. Vascular perfusion of cortical layers is correlated with neuron density in macaque striate cortex. Section cut perpendicular to the pial surface viewed under darkfield illumination provided by 2 planar fiberoptic flares crossed at 90°. Endogenous peroxidase activity in red blood cells appears golden orange. The strongest vascular signal is present in layers 2, 4c, and 6; the weakest signal is seen in layers 1, 4b, and 5.

peroxidase staining, giving the cortex a patchy appearance. Where the section passed into layer 4, large blood vessels became sparse and red blood cells were distributed more homogenously in the tissue. In layers 5 and 6 there also were few large blood vessel profiles, because only a minority of vessels descending from the pial surface reaches the infragranular cortex (Duvernoy et al. 1981).

At higher magnification, the largest penetrating blood vessels gave rise to small horizontal branches that bifurcated successively into the adjacent cortical tissue (Fig. 3*a*, 4*a*). There was a blush of peroxidase staining around each large vessel, owing to a lacy network of fine capillaries. Each large vessel was situated at the center of a ring consisting of more numerous, smaller vessels. The smaller vessels were each surrounded by a clear zone where capillaries were absent.

On the pial surface, the arterial and venous circulations could be differentiated by inspection (Fig. 3*b*). The arteries were densely packed with clotted blood, and hence appeared nearly black against the underlying neuropil. They had relatively thick walls, compared with their lumen diameters. The arteries formed a continuous vascular network over the pial surface. Therefore, once a main arterial trunk was identified, one could trace systematically the whole arterial plexus because the system was interconnected (Fig. 3*c*).

The pial veins were usually larger in diameter than the arteries, but they had thinner walls. They were often filled incompletely with erythrocytes and partially collapsed, presumably because blood drained into the dural venous sinuses at death. This made them appear more faintly labeled in comparison to the pial arteries (Fig. 3*b*). In regions where they were only partially filled, one could still follow their course across labeling gaps because of endogenous peroxidase activity in red blood cells clinging to the vein wall. In some areas the pial veins contained so few red cells that only the pial arterial system could be reconstructed. For identification of descending arterioles and venules, we selected regions where the pial arteries and veins were relatively well filled with blood.

The pial veins were not organized into a reticulum as were the arteries. Instead, they formed a drainage system like a river watershed, bifurcating into finer and finer tributaries that eventually ended at the site of each penetrating venule (Florey 1925; Hakim and Fisher 1957; Gillilan 1974; Duvernoy et al. 1981). The caliber of a pial venous branch often increased abruptly in size where it was fed by a penetrating venule that exited from the cortex.

It was possible to identify the sites on the brain surface at which vessels penetrated into the cortex from the pial arteries and veins (Fig. 3*c*). Once all the entry sites were mapped, their locations were superimposed upon a tangential section in layer 3 (Fig. 3*a*). Each surface penetration site coincided with a major vessel profile in layer 3, because blood vessels follow a radial course as they descend through the cortical layers. This approach permitted positive identification of each vessel profile in deeper sections as either a venule or arteriole (Fig. 3*d*). The larger vessels at the center of each capillary plexus proved to be venules. Occasionally, venules were located adjacent to each other, but usually they were separated by an intervening arteriole. In this example there were 50 venules in a region measuring 11.4 mm^2, indicating that each microvascular lobule serves 0.22 mm^2 of striate cortex. This is close to the reported value of one CO patch per 0.20 mm^2 cortex (Horton 1984).

The smaller vessels forming the perimeter of each microvascular lobule were found to be arterioles by matching with the pial vasculature. Each arteriole was silhouetted by a pale, capillary-free zone for a radius of ~50 μm. This characteristic feature was identified by Pfeifer (1930) as a "Zirkumvasaler Kapillarfreier Raum." It is not clear if he realized that a circumvascular capillary free space is a more prominent feature of arterioles than venules. Presumably it occurs around arterioles because the diffusion of molecules occurs for some distance with sufficient efficiency that capillaries are unnecessary.

Figure 4*a* shows a single microvascular lobule, consisting of a central venule and a wreath of 6 surrounding arterioles. The majority of red blood cells were concentrated in the central venule and nearby draining capillaries. The ring formed by the arterioles had a slightly lower overall density of red cells, due to the capillary free space around each arteriole. The dark labeling of the central venule, and the high concentration of red blood cells in its immediate vicinity, were responsible for the punctuate appearance of the peroxidase label in tangential sections viewed at low power (Fig. 2*a*).

Figure 4*b* shows the corresponding penetration sites in pial vessels used to establish the identity of each blood vessel profile as either arteriole or venule. Penetrating arterioles usually arose from small branches running between major arterial trunks or from short, dead-end twigs. There was often a focal constriction at the origin of a small pial arterial branch, suggesting the presence of a vascular sphincter (Fig. 4*b*).

Comparison of Microvascular Lobules and CO Patches

The periodicity of the microvascular lobules was comparable to the spacing of the CO patches, giving the 2 patterns a strong resemblance (compare Fig. 2*a* and *b*). To test the exact relationship between microvascular lobules and CO patches, the latter were delineated by thresholding CO activity, with the densest third of pixels defined as patches (Fig. 5*a* and *b*). The outlines of the CO patches were transferred onto the mosaic of microvascular lobules, using blood vessels for precise alignment. Although the microvascular lobules and CO patches had a similar periodicity, by inspection there was no tendency for them to overlap more often than one would expect by chance (Fig. 5*c*). The

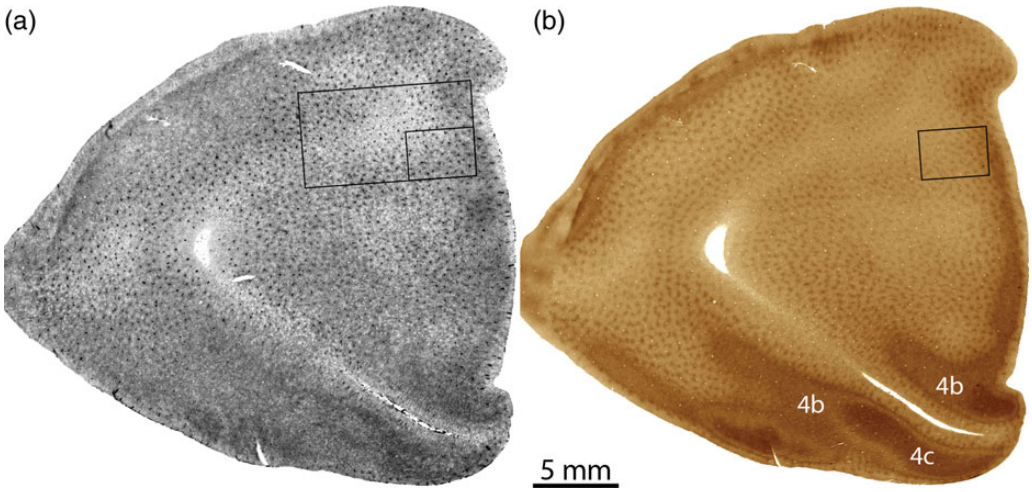

Figure 2. The vascular supply of the cerebral cortex is organized into microvascular lobules in the supragranular layers. (*a*) In Monkey 1 a section cut tangentially to the pial surface shows a regular, punctuate distribution of DAB label in layer 2/3 of the left operculum corresponding to red blood cells. Boxed regions are analyzed quantitatively in Figs. 3a, 5c, and 6. (*b*) Adjacent section reacted for CO reveals the patches. The lower portion of the section passes into layer 4, where the microvascular lobules are not present. Note the similar periodicity of microvascular lobules and CO patches. Boxed region is shown in Fig. 5a.

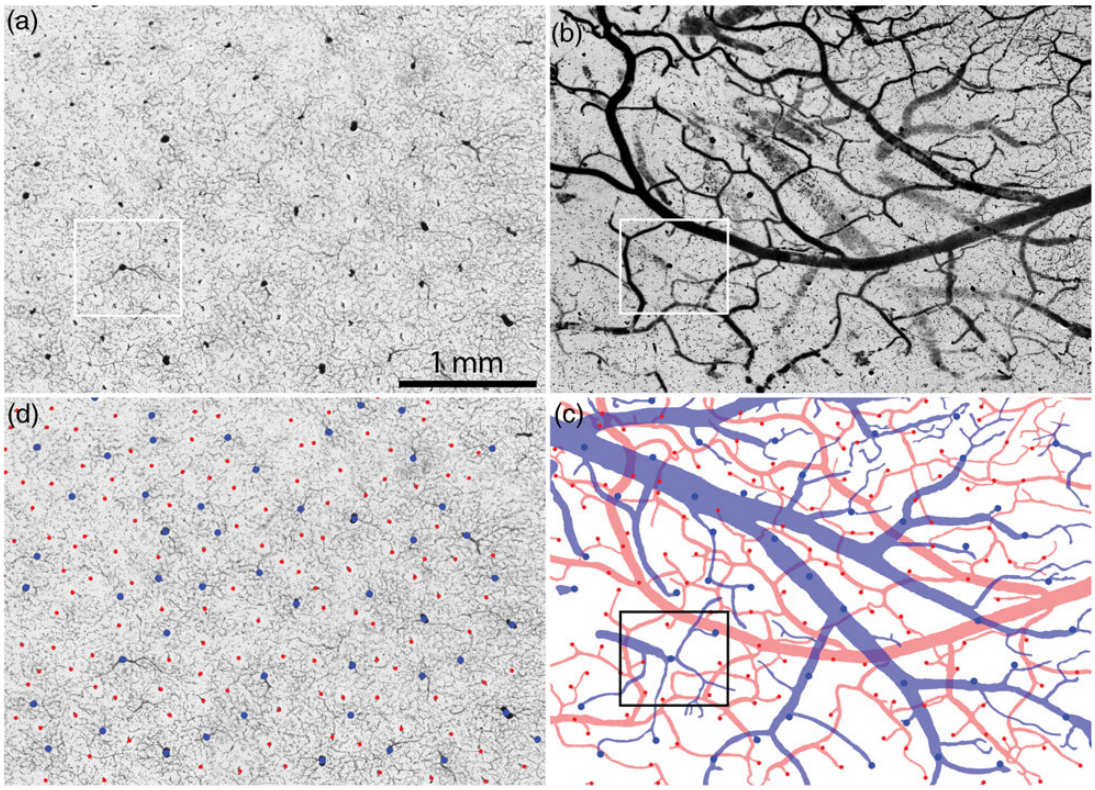

Figure 3. Identification of venules and arterioles in layer 3 by alignment with the pial vasculature. (*a*) Small boxed region in Fig. 2a showing blood in the cortical circulation. Larger vessels are surrounded by a dense capillary plexus, whereas smaller vessels are ringed by a clear zone where capillaries are absent. (*b*) 150 μm section from the surface of the cortical block, containing the pial arteries and veins. The veins are larger, but less well filled. (*c*) Drawing of the arterial (red) and venous (blue) pial circulations, with vessel penetration sites marked with colored spots. The veins form a drainage system while the arteries are organized into an anastomotic plexus. (*d*) Penetration sites in (*c*) superimposed on the image in (*a*), to identify arterioles and venules.

microvascular lobules, each drained by a large central vein, did not tend to coincide spatially with the CO patches.

The relationship between the microvascular lobules and the CO patches was examined quantitatively in 2 ways. First, the distribution of penetrating vessels was mapped. In each monkey, the sites of vessels penetrating from the pial vasculature were plotted over a wide area (Fig. 2*a*) to categorize vessel profiles in layer 3 as either arterioles or venules. In Monkey 1, a region measuring 55.8 mm^2 contained 770 arterioles and 306 venules (2.52:1). There were 242/770 (31.4%) arterioles and 106/306 (34.6%) venules located in CO patches (Fig. 6). This was not significantly different from the 33.3% proportion expected

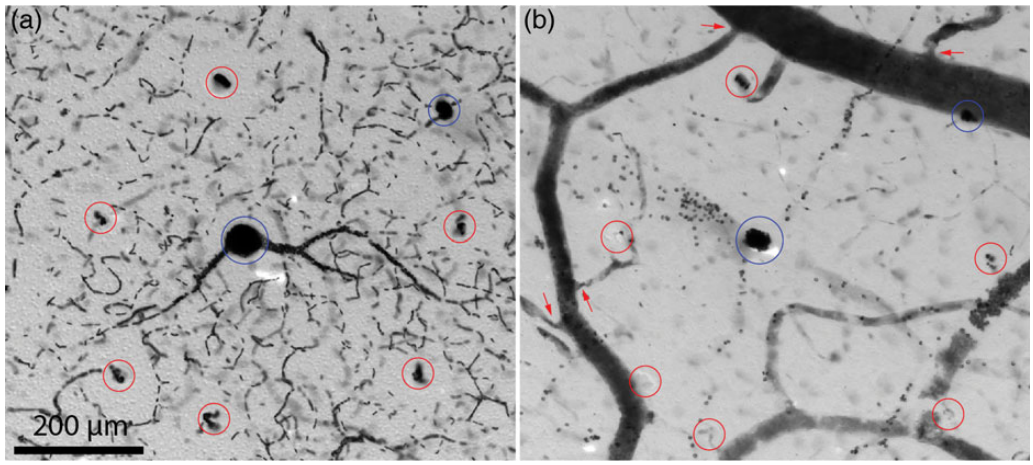

Figure 4. Single microvascular lobule in layer 3. (*a*) Boxed region in Fig. 3a showing a central venule (blue circle) surrounded by 6 arterioles (red circles). Mean distance from arterioles to central venule is 280 μm. There is another venule at the upper right, belonging to an adjacent microvascular lobule. (*b*) Boxed region in Fig. 3b showing 6 penetration sites (red circles) from surface pial arterioles wreathing a penetration site (blue) from a pial vein. In the microscope, varying the focus brings the cut edges of each penetration site into sharper view. Arrows show narrowing of arterioles as they branch from larger trunks, representing potential sphincter sites for control of local blood flow into the cortex.

by chance (χ^2 test two-sided P value = 0.26 for arterioles and 0.63 for venules). In Monkey 2, an area measuring 50.0 mm^2 had 526 arterioles and 199 venules (2.64:1). Fewer vessels were categorized than in Monkey 1, because the pial vasculature was less completely labeled. There were 179/526 (32.3%) arterioles and 67/199 venules (31.7%) located in patches (Fig. 6). Again, the percentage of arterioles and venules located in patches was not significantly different from 33.3% (P = 0.74 for arterioles and 0.92 for venules).

Second, the distribution of red blood cells with respect to CO patches was tested. Most of the red cells in the cortex were located in capillaries. These vessels are difficult to count or measure because they are very small, numerous, and sectioned at random angles. To assess the spatial overlap between CO patches and the whole vascular bed, the grayscale values were summed for all pixels located within CO patches in a layer 3 DAB section. The total was compared with the sum of grayscale values for pixels located in interpatches. In Monkey 1, the values were 29 884 876 (32%) for patches and 64 014 390 (68%) for interpatches. As a control, rotating the patch mosaic by 180° resulted in 34% of pixels in patches and 66% in interpatches. In Monkey 2, the summed grayscale values were 28 734 359 (33%) for patches and 58 719 844 (67%) for interpatches. The close match between the percentages of summed pixel grayscale values and the patch/interpatch areas (33/67) indicates that red blood cells were distributed randomly with respect to CO patches, at least in layer 3. It should be noted that the pixel grayscale density value includes contributions from red cells in arterioles, venules, and capillaries. Given that direct counts showed that arterioles and venules have no predilection for patches (Fig. 6), one can infer that the capillary bed associated with each microvascular lobule also lacks any affinity for patches.

If the arterioles were arrayed in a perfect hexagonal lattice, with a venule in the center of each lobule, the ratio of arterioles/venules would be 2:1. In fact, the vascular microlobules form a rather irregular, quasi-hexagonal array with a mean ratio of 2.58 arterioles per venule.

Combining data from the 2 animals, the mean arteriole diameter was 36.0 ± 10.0 μm (n = 421) in patches and 35.2 ± 10.0 μm (n = 875) in interpatches. The 95% confidence intervals overlapped for arteriole size in patches (35.1, 37.0 μm) versus interpatches (34.5, 35.9 μm). The mean venule diameter was 47.3 ± 15.9 μm (n = 173) in patches and 45.8 ± 15.5 μm (n = 332) in interpatches. The 95% confidence intervals for venule size in patches (44.9, 49.7 μm) and interpatches (44.1, 47.5 μm) also overlapped.

Combining patches and interpatches, the mean venule diameter (46.4 ± 15.7 μm) was significantly larger than the mean arteriole diameter (35.5 ± 10.0 μm) (P < 0.0001). On average there was one major penetrating venule, and hence one microvascular lobule, per 0.21 mm^2 cortex. There was one penetrating arteriole per 0.082 mm^2.

Shared Origin of Blood Supply to Patches and Interpatches

To learn if patches and interpatches share the same blood supply, the pial arterial circulation was examined over a wide expanse of cortex (Fig. 7*a*). The CO patches were labeled in a deeper section through layer 3 (Fig. 7*b*). Each surface arteriole penetration site was matched to a corresponding blood vessel profile in the CO section. As mentioned earlier, the surface arteries formed a highly anastomotic plexus. The arterioles that supplied patches were derived from the same segments of surface arteries that supplied interpatches (Fig. 7*c*). There was no evidence for segregated pial arterial circulations, one for patches and the other for interpatches. In this example, 174/502 arterioles supplied patches, a proportion (34.7%) that did not differ significantly from the distribution (33%) expected by chance (P = 0.63).

Discussion

The primary sensory areas are comprised of koniocortex, defined by a dense concentration of cells within the inner granular layer. In the primary visual cortex, this layer—known as 4c—is perfused by an elaborate capillary bed (Fig. 1) (Bell and Ball 1985; Fonta and Imbert 2002; Weber et al. 2008). Layer 4c is so heavily vascularized that it can be resolved by high-resolution functional magnetic resonance imaging (Goense and Logothetis 2006; Goense et al. 2012). Not coincidentally, layer 4c receives the bulk of the lateral geniculate body's projection and displays the highest level of CO activity. In contrast, cell sparse layers such as 4b and 5, which receive no geniculate input, have a

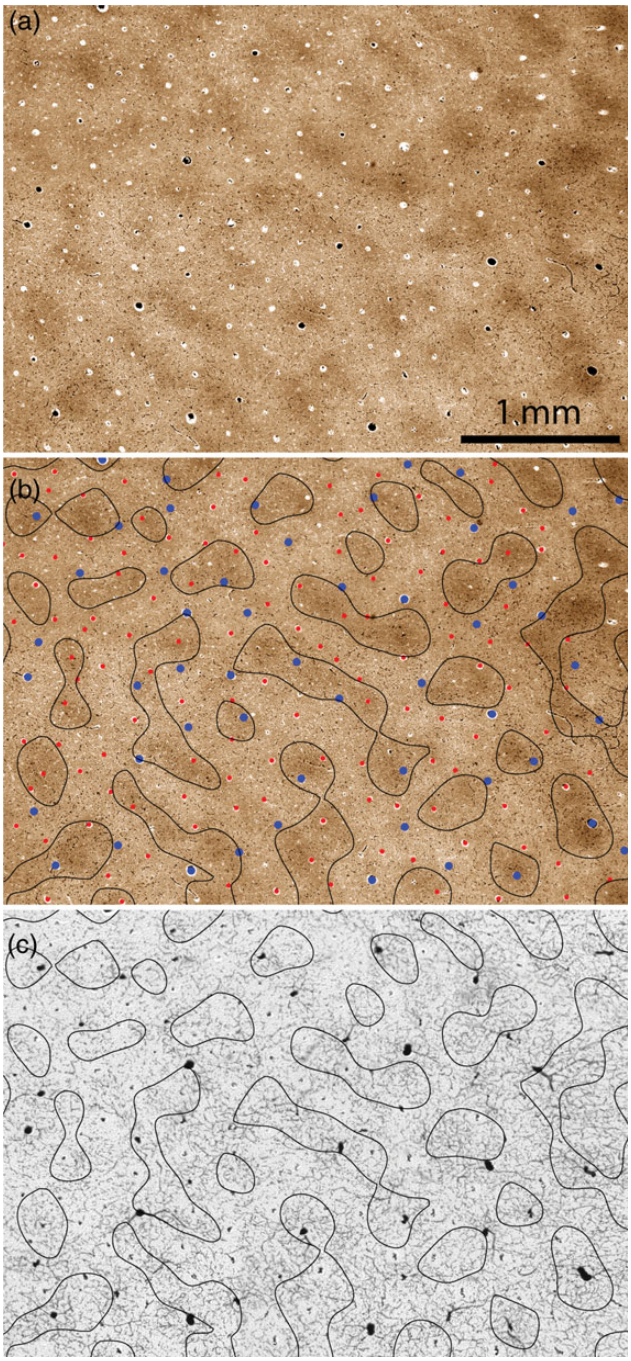

Figure 5. Relationship between microvascular lobules and CO patches. (*a*) CO patches from the boxed region in Fig. 2b. (*b*) Borders of the CO patches in (*a*) defined by thresholding the darkest one-third of pixels, with the blood vessels identified as either arterioles (red) or venules (blue) from the adjacent section in Fig. 3d. (*c*) Borders of the CO patches in (*b*) superimposed on the microvascular lobules shown in Fig. 3a. There is no coincidence between the vascular system and the CO patches.

relatively meager blood supply. Cell density, thalamic input, and metabolic activity all correlate with the laminar structure of cortical blood flow (Duret 1874; Dunning and Wolff 1937; Craigie 1945; Lierse 1963; Duvernoy et al. 1981; Hirsch et al. 2012). However, the coupling is not perfect, because layer 4a has no counterpart in the microvascular system, despite having robust CO activity and direct geniculate input.

It has been more difficult to determine if the vascular supply of the cerebral cortex is specialized with respect to its

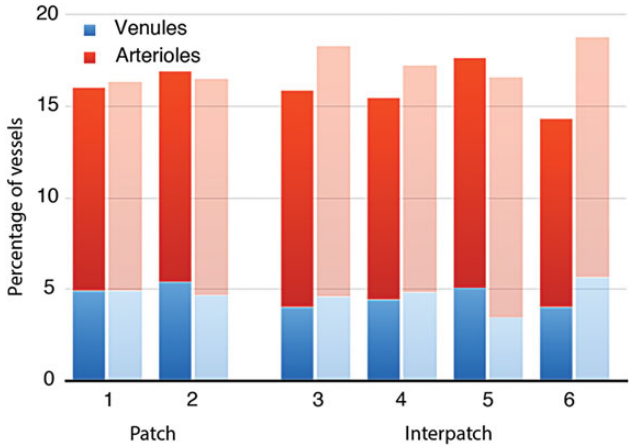

Figure 6. Distribution of venules and arterioles in patches versus interpatches. Histograms showing percentage of vessels in patches versus interpatches for Monkey 1 ($n = 1076$, darker shading) and Monkey 2 ($n = 725$, lighter shading). CO activity was divided into 6 density zones of equal area, with the darkest 2 designated as patches. For each animal, a third of the vessels were located in patches, and the ratio of arterioles/venules showed no trend across the 6 CO density compartments.

columnar architecture, partly because no reliable labeling method exists to classify radial blood vessel profiles as arterioles or venules. To solve this problem we mapped the dive down points where blood vessels from the leptomeningeal arteries and veins penetrate the cortex (Fig. 3). These were matched to individual vessel profiles in layer 3 to establish their identity. This approach permitted delineation of the cortical microvascular lobules, each consisting of a major venule draining a capillary plexus that is supplied by a surrounding ring of arterioles (Duvernoy et al. 1981).

One would expect CO patches to have a greater blood supply because (1) their neurons have higher average discharge rates, (2) they receive a direct koniocellular geniculate projection, and (3) they contain increased levels of metabolic enzymes. This prediction was not borne out by our findings. Although microvascular lobules and CO patches have a similar periodicity, they have no tendency to overlap (Fig. 5). With one-third of the surface area of striate cortex allocated to patches, one-third of the penetrating arterioles and venules are located in patches (Fig. 6). If microvascular lobules had a systematic relationship with CO patches, the latter would contain a disproportionate fraction of the arterioles or venules, depending on the phase alignment between the 2 structures. For example, if microvascular lobules were centered on CO patches, the majority of large penetrating veins would be located in patches.

No difference was found in the density or caliber of penetrating vessels in patches versus interpatches. It was not the case that vessels in CO patches had a larger bore, making them capable of delivering more erythrocytes. Conceivably, microvascular lobules that overlap with CO patches might be endowed with a more extensive capillary plexus than those situated in interpatch zones. To address this point we compared summed image pixel values for DAB labeling in patches versus interpatches. This analysis revealed no disproportionate red blood cell signal coinciding with the CO patches. A potential weakness of our method is that the distribution of red cells in the tissue after death might differ from the distribution present during life. It seems rather unlikely that a systematic transfer of red cells from patches to interpatches would occur upon death, although we cannot rule out this possibility.

Two prior studies have addressed the vascularity of CO patches by measuring blood vessel density in perfused tissue. Zheng et al. (1991) manually drew the "microvessels" in CO-stained tangential sections. They reported that the total length/mm^2 was 42% greater in patches than interpatches. A potential explanation for this finding is that empty capillaries are more visible, and hence easier to draw, in regions where background CO staining is dark. When the authors performed a control analysis by tracing vessel profiles in unstained sections, the increased vascularity of patches was less evident.

In a recent study, Keller et al. (2011) also found a significant difference in vascularity between patch and interpatch regions. The density of small, horizontally coursing vessels, which are mostly capillaries, was 4.4% greater in patches than in interpatches. The disagreement with our findings may reflect our differing methods. We labeled red cells and simply compared their optical density in patches versus interpatches. Keller et al. examined perfused tissue and quantified blood vessels, not blood cells. CO sections were double-labeled using fluorescence immunohistochemistry for collagen to visualize blood vessels. Thresholded images were skeletonized to yield single-pixel wide traces of vessels, their lengths were summed, and then converted to mm vessel/mm^3 tissue after compensating for section thickness. Given such disparate approaches, the discrepancy between a 4.4% increase in capillary density in patches (Keller's result) and no increase (our result) is minor.

Our data are discrepant on another point, which is harder to dismiss. Keller et al. (2011) reported 17.6% more penetrating vessels in interpatches than patches. It is puzzling to conceive of a cortical vascular system comprised of more large vertical vessels in interpatches but more capillaries in patches. Our data showed the same density of perpendicular vessels in patches and interpatches (Fig. 6).

A potential explanation for these conflicting results is that Keller et al. drew the patch borders by visual inspection. In tangential sections, CO staining is lighter in layer 2 than in layer 3. As a result, when judging by eye the patches appear smaller in layer 2 (Fig. 8). Duvernoy et al. (1981) identified 5 groups of penetrating cortical blood vessels. Type 1 vessels descend only to layer 2. These vessels are small and difficult to inject with gelatin, hence Duvernoy did not hazard a guess as to the fraction they represent. Nonetheless, it is clear that small penetrating vessel profiles are more abundant in layer 2 than layer 3 (Fig. 8). Consequently, if more tissue is allocated to interpatches in layer 2 than in layer 3, measurements will yield: (1) a higher vessel density in interpatches and (2) a skew towards smaller vessel diameters in interpatches. Both these results were reported (see Fig. 4, Keller et al. 2011).

Much of the brain's vascular system forms during fetal life, but considerable elaboration and remodeling of vessels occur during postnatal life (Harb et al. 2013). In the macaque, CO

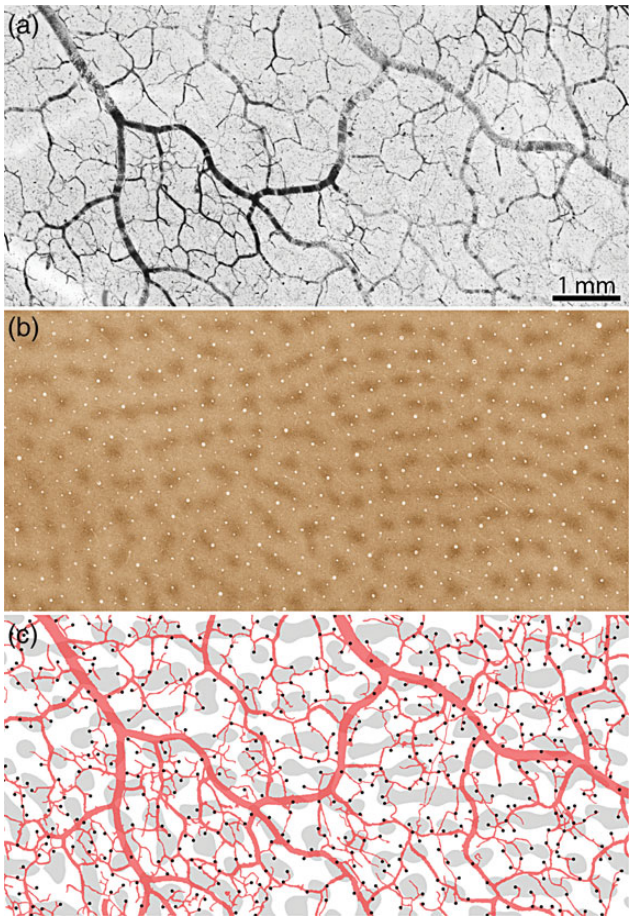

Figure 7. United arterial supply to patches and interpatches. (*a*) Pial arterial vessels in Monkey 2, from a region where the surface veins were not filled. (*b*) CO patches in layer 3 from the same region. (*c*) Drawing of the surface vessels superimposed on the thresholded CO patches, marking each arteriole penetration site (dark spots). The pial arteries form a highly anastomotic system, with patches and interpatches supplied by shared portions of the vascular reticulum.

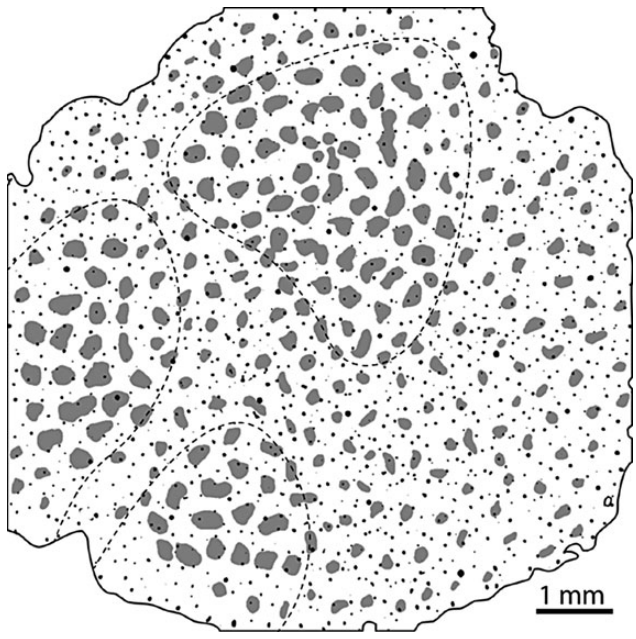

Figure 8. Differences between layer 2 and layer 3 can affect measurement of blood vessel density and size. Thresholded CO-stained section of monkey visual cortex (after Fig. 1, Keller et al. 2011, p. 1248) showing blood vessels as small black dots. Their overall density is 27.4 vessels/mm^2, near to Keller's reported value of 28.2 vessels/mm^2. Vessel density is greater in layer 2 (30.1 vessels/mm^2) than in layer 3 (23.6 vessels/mm^2). CO staining is also lighter in layer 2 than in layer 3 (within dashed lines). Consequently, one tends to draw smaller patches (grey shading) in layer 2 than in layer 3. Delineating smaller patches in layer 2, a layer with a higher density of small blood vessels, skews the interpatch/patch ratio of blood vessels in the whole-tissue section. In this example there are 28.2 vessels/mm^2 in interpatches and 23.9 vessels/mm^2 in patches, replicating the 1.18:1 ratio reported by Keller et al. (2011).

patches, ocular dominance columns, and orientation columns develop in utero (Wiesel and Hubel 1974; Horton 1984; Horton and Hocking 1996), but refinement continues during a critical period of cortical plasticity after birth. Therefore, cortical columns and blood vessels overlap in their developmental timetable. One cannot attribute the lack of a relationship to a mismatch in the timing of their maturation.

The rodent barrelfield is another area where the relationship between blood supply and functional architecture has been examined. Endovascular casts have shown a separate tuft of capillaries supplying each whisker barrel, implying a specialized vasculature (Cox et al. 1993; Woolsey et al. 1996). In addition, perturbed sensory experience through whisker manipulation has been shown to alter capillary density in barrels (Whiteus et al. 2014). Given that barrels contain cell dense and cell sparse zones, as do the cortical layers, it would not be a surprise to find associated fluctuations in local capillary density. However, a recent study has challenged the idea that barrels have a richer capillary supply (Blinder et al. 2013). In passing we note that a whisker barrel should probably not be regarded as a cortical column. It is more accurately described as an isomorphic representation of a peripheral organ, in this case, a cylindrical whisker follicle. In other words, barrels represent a form of somatotopic organization rather than columnar organization (Horton and Adams 2005).

It is possible to image microvascular lobules in animals using a contrast agent in conjunction with high magnetic field time-of-flight microangiography (Harel et al. 2010). A correlation between microvascular lobules and cortical columns would provide a useful tool for probing neural function with magnetic resonance imaging. Unfortunately, our data do not support such a correlation (Fig. 6). Moreover, penetrating arterioles are fed by a richly anastomotic system of surface vessels that does not discriminate between patches and interpatches (Fig. 7). However, Gardner's proposal for functional organization of the cortical vasculature is still tenable, if flow through penetrating arterioles is regulated by sphincters. We often observed focal constriction of the blood column in small pial branches (Fig. 4), as reported by others (Florey 1925; Rowbotham and Little 1962; Duvernoy et al. 1981; Harrison et al. 2002; Gordon et al. 2007; but see Weber et al. 2008). These putative sphincters appear to be innervated by the autonomic nervous system, potentially allowing neurogenic regulation of blood flow through individual penetrating arterioles (Baramidze et al. 1982, 1992). This feature could explain why cortical columns can be resolved with fMRI, despite the lack of any "hard-plumbed" relationship between columns and vessels. Presumably, activation of neurons in columns tuned to a particular stimulus leads to dilation of the sphincters controlling flow to individual penetrating arterioles (Peppiatt et al. 2006; Fernandez-Klett et al. 2010). The pial venous system, on the other hand, is not regulated by sphincters. The convergence of blood flow (Fig. 3*c*) would account for the presence of stimulus-specific signals in large surface veins (Boynton 2005; Shmuel et al. 2010; Sun et al. 2013).

How do neurons in CO patches sustain a 49% higher mean firing rate without a richer microcirculation? Perhaps in CO patches the rate of capillary blood flow is slightly faster or the oxygen extraction ratio is higher. It would be interesting to estimate how much these parameters would need to increase to satisfy the greater metabolic requirements of CO patches.

Funding

This work was supported by grants EY10217 (J.C.H.), EY02162 (Beckman Vision Center) from the National Eye Institute, and Research to Prevent Blindness. The California National Primate Research Center is supported by NIH Base Grant RR00169.

Notes

Technical support was provided by Valerie L. Wu and James V. Botelho. *Conflict of Interest*: None declared.

References

Atkins GB, Jain MK, Hamik A. 2011. Endothelial differentiation: molecular mechanisms of specification and heterogeneity. Arterioscler Thromb Vasc Biol. 31:1476–1484.

Baramidze D, McHedlishvili G, Gordeladze Z, Levkovitch Y. 1992. Cerebral microcirculation: heterogeneity of pial arterial network controlling microcirculation of cerebral cortex. Int J Microcirc Clin Exp. 11:143–155.

Baramidze DG, Reidler RM, Gadamski R, McHedlishvili GI. 1982. Pattern and innervation of pial microvascular effectors which control blood supply to cerebral cortex. Blood Vessels. 19:284–291.

Bell MA, Ball MJ. 1985. Laminar variation in the microvascular architecture of normal human visual cortex (area 17). Brain Res. 335:139–143.

Blinder P, Tsai PS, Kaufhold JP, Knutsen PM, Suhl H, Kleinfeld D. 2013. The cortical angiome: an interconnected vascular network with noncolumnar patterns of blood flow. Nat Neurosci. 16:889–897.

Bonhoeffer T, Grinvald A. 1991. Iso-orientation domains in cat visual cortex are arranged in pinwheel-like patterns. Nature. 353:429–431.

Boynton GM. 2005. Imaging orientation selectivity: decoding conscious perception in V1. Nat Neurosci. 8:541–542.

Cheng K, Waggoner RA, Tanaka K. 2001. Human ocular dominance columns as revealed by high-field functional magnetic resonance imaging. Neuron. 32:359–374.

Cox SB, Woolsey TA, Rovainen CM. 1993. Localized dynamic changes in cortical blood flow with whisker stimulation corresponds to matched vascular and neuronal architecture of rat barrels. J Cereb Blood Flow Metab. 13:899–913.

Craigie EH. 1945. The architecture of the cerebral capillary bed. Biol Rev. 20:133–146.

dela Paz NG, D'Amore PA. 2009. Arterial versus venous endothelial cells. Cell Tissue Res. 335:5–16.

DeYoe EA, Trusk TC, Wong-Riley MT. 1995. Activity correlates of cytochrome oxidase-defined compartments in granular and supragranular layers of primary visual cortex of the macaque monkey. Vis Neurosci. 12:629–639.

Dunning HS, Wolff HG. 1937. The relative vascularity of various parts of the central and peripheral nervous system of the cat and its relation to function. J Comp Neurol. 67:433–450.

Duret M. 1874. Recherches anatomiques sur la circulation de l'encéphale. Arch Physiol Norm Patholol. I:60–91, 316–353, 664–693, 919–957.

Duvernoy HM, Delon S, Vannson JL. 1981. Cortical blood vessels of the human brain. Brain Res Bull. 7:519–579.

Economides JR, Sincich LC, Adams DL, Horton JC. 2011. Orientation tuning of cytochrome oxidase patches in macaque primary visual cortex. Nat Neurosci. 14:1574–1580.

Farias MF, Gattass R, Piñón MC, Ungerleider LG. 1997. Tangential distribution of cytochrome oxidase-rich blobs in the primary visual cortex of macaque monkeys. J Comp Neurol. 386:217–228.

Fernandez-Klett F, Offenhauser N, Dirnagl U, Priller J, Lindauer U. 2010. Pericytes in capillaries are contractile in vivo, but arterioles mediate functional hyperemia in the mouse brain. Proc Natl Acad Sci USA. 107:22290–22295.

Florey H. 1925. Microscopical observations on the circulation of the blood in the cerebral cortex. Brain. 48:43–64.
Fonta C, Imbert M. 2002. Vascularization in the primate visual cortex during development. Cereb Cortex. 12:199–211.
Gardner JL. 2010. Is cortical vasculature functionally organized? Neuroimage. 49:1953–1956.
Gillilan LA. 1974. Potential collateral circulation to the human cerebral cortex. Neurology. 24:941–948.
Goense JB, Logothetis NK. 2006. Laminar specificity in monkey V1 using high-resolution SE-fMRI. Magn Reson Imaging. 24:381–392.
Goense J, Merkle H, Logothetis NK. 2012. High-resolution fMRI reveals laminar differences in neurovascular coupling between positive and negative BOLD responses. Neuron. 76:629–639.
Gordon GR, Mulligan SJ, MacVicar BA. 2007. Astrocyte control of the cerebrovasculature. Glia. 55:1214–1221.
Hakim S, Fisher C. 1957. A new technique for the microscopic examination of cerebral vessels in vivo. J Neurosurg. 14:405–412.
Harb R, Whiteus C, Freitas C, Grutzendler J. 2013. In vivo imaging of cerebral microvascular plasticity from birth to death. J Cereb Blood Flow Metab. 33:146–156.
Harel N, Bolan PJ, Turner R, Ugurbil K, Yacoub E. 2010. Recent advances in high-resolution MR application and its implications for neurovascular coupling research. Front Neuroenerg. 2:130.
Harrison RV, Harel N, Panesar J, Mount RJ. 2002. Blood capillary distribution correlates with hemodynamic-based functional imaging in cerebral cortex. Cereb Cortex. 12:225–233.
Hirsch S, Reichold J, Schneider M, Szekely G, Weber B. 2012. Topology and hemodynamics of the cortical cerebrovascular system. J Cereb Blood Flow Metab. 32:952–967.
Horton JC. 1984. Cytochrome oxidase patches: a new cytoarchitectonic feature of monkey visual cortex. Philos Trans R Soc Lond B Biol Sci. 304:199–253.
Horton JC, Adams DL. 2005. The cortical column: a structure without a function. Philos Trans R Soc Lond B Biol Sci. 360:837–862.
Horton JC, Hocking DR. 1996. An adult-like pattern of ocular dominance columns in striate cortex of newborn monkeys prior to visual experience. J Neurosci. 16:1791–1807.
Horton JC, Hubel DH. 1981. Regular patchy distribution of cytochrome oxidase staining in primary visual cortex of macaque monkey. Nature. 292:762–764.
Hubel DH, Wiesel TN. 1969. Anatomical demonstration of columns in the monkey striate cortex. Nature. 221:747–750.
Hubel DH, Wiesel TN. 1977. The Ferrier Lecture: functional architecture of macaque monkey visual cortex. Proc R Soc Lond B Biol Sci. 198:1–59.
Hubel DH, Wiesel TN, Stryker MP. 1978. Anatomical demonstration of orientation columns in macaque monkey. J Comp Neurol. 177:361–380.
Hübener M, Shoham D, Grinvald A, Bonhoeffer T. 1997. Spatial relationships among three columnar systems in cat area 17. J Neurosci. 17:9270–9284.
Issa NP, Trepel C, Stryker MP. 2000. Spatial frequency maps in cat visual cortex. J Neurosci. 20:8504–8514.
Kamitani Y, Tong F. 2005. Decoding the visual and subjective contents of the human brain. Nat Neurosci. 8:679–685.
Kapralov A, Vlasova II, Feng W, Maeda A, Walson K, Tyurin VA, Huang Z, Aneja RK, Carcillo J, Bayir H et al. 2009. Peroxidase activity of hemoglobin–haptoglobin complexes: covalent aggregation and oxidative stress in plasma and macrophages. J Biol Chem. 284:30395–30407.
Keller AL, Schuz A, Logothetis NK, Weber B. 2011. Vascularization of cytochrome oxidase-rich blobs in the primary visual cortex of squirrel and macaque monkeys. J Neurosci. 31:1246–1253.
Kety SS. 1948. Quantitative determination of cerebral blood flow in man. Methods Med Res. 1:204–217.
Lawrence W. 1819. Lectures on the physiology, zoology, and the natural history of man. London: J. Callow, p. 105.
LeVay S, Nelson SB. 1991. Columnar organization of the visual cortex. In: Leventhal AG, editor. The neural basis of visual function. Boston: CRC Press, p. 266–p. 315.
Lierse W. 1963. Die Kapillardichte im Wirbeltiergehirn. Acta Anat (Basel). 54:1–31.
Logothetis NK, Wandell BA. 2004. Interpreting the BOLD signal. Annu Rev Physiol. 66:735–769.
Lu HD, Roe AW. 2008. Functional organization of color domains in V1 and V2 of macaque monkey revealed by optical imaging. Cereb Cortex. 18:516–533.
Marcelo KL, Goldie LC, Hirschi KK. 2013. Regulation of endothelial cell differentiation and specification. Circ Res. 112:1272–1287.
Mountcastle VB. 1997. The columnar organization of the neocortex. Brain. 120:701–722.
Peppiatt CM, Howarth C, Mobbs P, Attwell D. 2006. Bidirectional control of CNS capillary diameter by pericytes. Nature. 443:700–704.
Pfeifer RA. 1930. Grundlegende Untersuchungen für die Angioarchitektonik des menschlichen Gehirns. Berlin: von Julius Springer.
Purves D, LaMantia A. 1993. Development of blobs in the visual cortex of macaques. J Comp Neurol. 334:169–175.
Rowbotham GF, Little E. 1962. The circulations and reservoir of the brain. Br J Surg. 50:244–250.
Shen Z, Lu Z, Chhatbar PY, O'Herron P, Kara P. 2012. An artery-specific fluorescent dye for studying neurovascular coupling. Nat Methods. 9:273–276.
Shmuel A, Chaimow D, Raddatz G, Ugurbil K, Yacoub E. 2010. Mechanisms underlying decoding at 7 T: ocular dominance columns, broad structures, and macroscopic blood vessels in V1 convey information on the stimulated eye. Neuroimage. 49:1957–1964.
Sincich LC, Horton JC. 2005. Input to V2 thin stripes arises from V1 cytochrome oxidase patches. J Neurosci. 25:10087–10093.
Sun P, Gardner JL, Costagli M, Ueno K, Waggoner RA, Tanaka K, Cheng K. 2013. Demonstration of tuning to stimulus orientation in the human visual cortex: a high-resolution fMRI study with a novel continuous and periodic stimulation paradigm. Cereb Cortex. 23:1618–1629.
Swindale NV, Shoham D, Grinvald A, Bonhoeffer T, Hubener M. 2000. Visual cortex maps are optimized for uniform coverage. Nat Neurosci. 3:822–826.
Tootell RB, Silverman MS, De Valois RL. 1981. Spatial frequency columns in primary visual cortex. Science. 214:813–815.
Ts'o DY, Zarella M, Burkitt G. 2009. Whither the hypercolumn? J Physiol. 587:2791–2805.
Valverde Salzmann MF, Bartels A, Logothetis NK, Schuz A. 2012. Color blobs in cortical areas V1 and V2 of the new world monkey *Callithrix jacchus*, revealed by non-differential optical imaging. J Neurosci. 32:7881–7894.
Weber B, Keller AL, Reichold J, Logothetis NK. 2008. The microvascular system of the striate and extrastriate visual cortex of the macaque. Cereb Cortex. 18:2318–2330.
Whiteus C, Freitas C, Grutzendler J. 2014. Perturbed neural activity disrupts cerebral angiogenesis during a postnatal critical period. Nature. 505:407–411.
Wiesel TN, Hubel DH. 1974. Ordered arrangement of orientation columns in monkeys lacking visual experience. J Comp Neurol. 158:307–318.
Wong-Riley MTT. 1979. Changes in the visual system of monocularly sutured or enucleated cats demonstrable with cytochrome oxidase histochemistry. Brain Res. 171:11–28.
Woolsey TA, Rovainen CM, Cox SB, Henegar MH, Liang GE, Liu D, Moskalenko YE, Sui J, Wei L. 1996. Neuronal units linked to microvascular modules in cerebral cortex: response elements for imaging the brain. Cereb Cortex. 6:647–660.
Xu X, Bosking W, Sary G, Stefansic J, Shima D, Casagrande V. 2004. Functional organization of visual cortex in the owl monkey. J Neurosci. 24:6237–6247.
Yoshioka T, Blasdel GG, Levitt JB, Lund JS. 1996. Relation between patterns of intrinsic lateral connectivity, ocular dominance, and cytochrome oxidase-reactive regions in macaque monkey striate cortex. Cereb Cortex. 6:297–310.
Zheng D, LaMantia AS, Purves D. 1991. Specialized vascularization of the primate visual cortex. J Neurosci. 11:2622–2629.